

Reactivity of Pb(II) at the Mn(III,IV) (Oxyhydr)Oxide–Water Interface

CHRISTOPHER J. MATOCHA,^{*,†}
EVERT J. ELZINGA,[‡] AND
DONALD L. SPARKS[‡]

Department of Agronomy, University of Kentucky,
N-122 Agricultural Science Building-North,
Lexington, Kentucky 40546-0091, and
Department of Plant and Soil Sciences,
University of Delaware, Newark, Delaware 19717-1303

In this study, the reactivity of lead (Pb(II)) on naturally occurring Mn(III,IV) (oxyhydr)oxide minerals was evaluated using kinetic, thermodynamic, and spectroscopic investigations. Aqueous Pb(II) was more strongly adsorbed to birnessite (δ -MnO_{1.7}) than to manganite (γ -MnOOH) under all experimental conditions. The isothermic heat of Pb adsorption (ΔH_T) on birnessite was 94 kJ mol⁻¹ at a surface loading of 1.1 mmol g⁻¹, and decreased with increasing adsorption density. This indicated that adsorption was an endothermic process and that birnessite possessed heterogeneous sites of reactivity for Pb. X-ray absorption fine structure (XAFS) spectra revealed that Pb was adsorbed as inner-sphere complexes on both birnessite and manganite with no evidence to suggest oxidation as an operative sorption mechanism. Lead appeared to coordinate to vacancy sites in the birnessite layer structure with concurrent release of Mn to solution, which resulted in a greater number of second shell Mn scatterers in Pb–birnessite when compared to Pb–manganite samples. The difference in Pb coordination apparently explained the contrasting desorption behavior between the two Mn minerals. These results have significant implications for Pb partitioning in soil environments containing solid-phase Mn(III,IV) (oxyhydr)oxides.

Introduction

Environmental concerns over Pb(II) contamination in soils, sediments, and aquatic settings has given rise to the development of remediation strategies targeted at reducing the solubility and toxicity of Pb(II). As Pb(II) is generally associated with insoluble mineral phases, or bound through sorption processes in contaminated soils (1), the proposed strategies have focused on decreasing the solubility of Pb(II) through partitioning to solid-phase minerals (2–6) and through phytoremediation (7). Understanding the reactivity of soil components with Pb is necessary to predict the fate and transport of Pb in the environment and to optimize remediation efforts. This requires combining macroscopic and spectroscopic techniques to obtain mechanistic information (8, 9).

Sorption mechanisms of Pb on clays and oxides are complex. Strawn et al. (6), employing X-ray absorption

spectroscopy (XAS), noted that Pb sorbed as an inner-sphere bidentate surface complex on γ -Al₂O₃ with no evidence to suggest surface precipitation. Bargar et al. (10) conducted grazing-incidence XAS studies and showed that both outer-sphere and inner-sphere surface complexes occur between Pb and surface functional groups on α -Al₂O₃ depending on the specific surface site exposed. The uptake of Pb on goethite was enhanced in the presence of Cl⁻ due to Pb–Cl⁻–Fe(s) ternary complex formation based on XAFS-derived Pb–Fe distances (11). Other studies using 2:1 phyllosilicate minerals with fixed structural charge have reported metal exchange on basal planes and inner-sphere surface complexation at edge sites for Pb depending on ionic strength and pH (12).

The reactivity of Pb at the Mn(III,IV) (oxyhydr)oxide–water interface is not clearly understood. The phyllo-managanates or the birnessite group minerals possess low points of zero charge (PZC), and are typified by high specific surface areas, which endow them with significant surface reactivity (13). Thus, they can drastically affect surface charge characteristics of bulk field soils (14). It has been shown that birnessite has a disproportionately high sorption capacity for Pb, despite its low relative abundance in soils (15–17). Gatte and Laitinen (16) suggested that the high affinity of Pb for hydrous manganese dioxide over a wide pH range was attributed to oxidation of Pb(II) to Pb(IV) (as PbO₂) by MnO₂, a suggestion supported by other findings (18, 19). McKenzie (17) argued that strong specific (inner-sphere) binding accounted for the Pb(II) sorption behavior on birnessite. In the above-mentioned studies, only macroscopic observations were reported. Manceau et al. (20) presented the first XAS evidence for Pb reacted with birnessite and reported that Pb formed multinuclear surface complexes with birnessite. Recent XAS investigations reported Mn as a next-nearest neighbor in the second shell after reacting Pb with birnessite (21, 22).

To our knowledge, there is little information available linking spectroscopic data with kinetic and thermodynamic studies of the Pb–birnessite interface which is necessary because birnessite is the most commonly identified Mn oxide mineral in soils (13). The reactivity of a naturally occurring solid Mn(III) mineral with Pb(II), such as manganite (γ -MnOOH), has not been investigated, although it is a better solid-phase oxidant than birnessite at pH < 6 (23). The present study was undertaken to further examine Pb(II) reactivity at the Mn(III,IV) (oxyhydr)oxide–water interface through thermodynamic, kinetic, and spectroscopic studies.

Experimental Section

Materials. Birnessite (δ -MnO_{1.7}) was prepared according to procedures outlined by McKenzie (24). Measured BET surface area of birnessite was 40 m² g⁻¹, iodometrically determined oxidation state was 3.44, and powder X-ray diffraction *d* spacings confirmed the presence of synthetic birnessite. The pH at the point of zero charge (PZC) was estimated by measuring microelectrophoretic mobilities as a function of pH (25). Extrapolation of particle mobilities to zero revealed a PZC of 1.81 ± 0.04. Manganite (γ -MnOOH) was synthesized by oxidizing Mn(II) (as MnSO₄) with 30% H₂O₂ and forcing precipitation with 0.2 M NH₃ (26). The product was characterized by the same methods used for birnessite. The procedure produced a crystalline manganite based on sharp XRD peaks, mean oxidation state of 3.02, BET surface area of 32 m² g⁻¹, and an estimated PZC of 6.3 ± 0.06.

Reactivity Experiments. Lead sorption kinetic studies were conducted in batches using the pH-stat technique. For birnessite, rate studies were investigated at pH 3.5 in 0.01 M

* Corresponding author phone: (859) 257-9312; fax: (859) 257-2185; e-mail: cjmato2@pop.uky.edu.

[†] University of Kentucky.

[‡] University of Delaware.

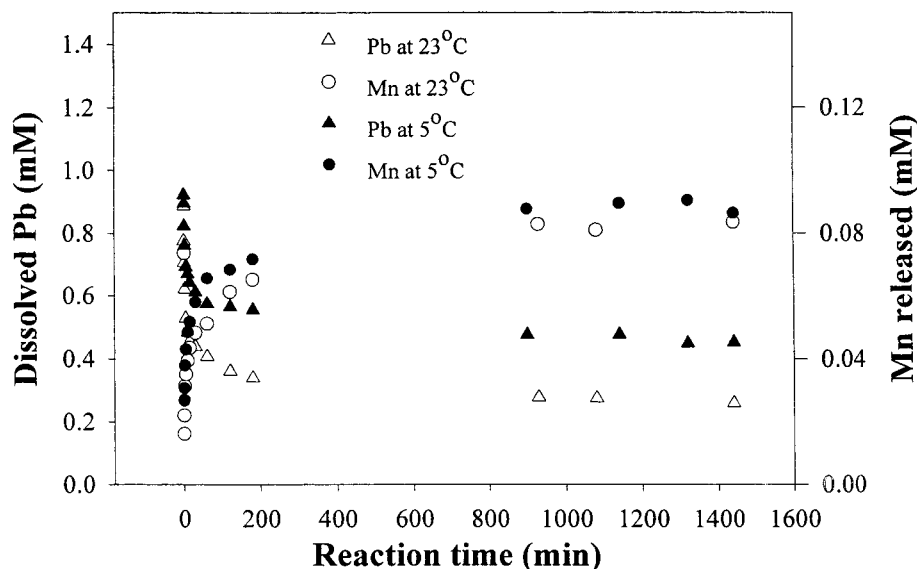


FIGURE 1. Pb(II) sorption kinetics and dissolved Mn release on 1 g L⁻¹ birnessite at pH 3.5, I = 0.01M NaClO₄, and [Pb]₀ = 1.9 mM, as a function of temperature.

NaClO₄, an initial Pb concentration of 1.9 mM, and 1.0 g L⁻¹. Under these conditions, MINEQL⁺ indicates the predominant Pb species to be 98.4% free Pb²⁺(aq) and 1.6% PbHCO₃⁺(aq). Kinetic experiments of Pb on manganite were measured at pH 6.7 in a glovebox under conditions that were undersaturated with respect to Pb-bearing solid phases (91.2% free Pb²⁺ and 8.8% PbOH⁺ at an initial Pb concentration of 14 μM). Aliquots of Pb were added from a 0.1 M Pb(ClO₄)₂ stock solution. Release rates of Mn were also followed to check for metal-promoted dissolution of the solid phase.

The pH-edge experiments were conducted at ionic strengths of 0.1 and 0.01 M NaClO₄ in a glovebox (to prevent possible precipitation of PbCO₃) under N₂ with boiled DI water at 296 K and 1 g L⁻¹ birnessite and 0.1 g L⁻¹ manganite. Adsorption isotherms of Pb on birnessite were determined using the batch equilibration method at 278 and 296 K using 1 g L⁻¹ at pH 3.5. Isotherms describing Pb adsorption were measured on 0.1 g L⁻¹ manganite in the glovebox at pH 6.7. Both sorbents were preequilibrated at the desired pH in 0.01 M NaClO₄ overnight before aliquots were transferred to centrifuge tubes and spiked with appropriate aliquots of a 0.1 M Pb stock solution to achieve initial Pb concentrations ranging from 9.6 × 10⁻⁶ to 1.5 × 10⁻³ M. The strong pH dependence of Pb uptake on manganite necessitated the use of 5 mM MES [2-(N-morpholino)ethane sulfonic acid] buffer, adjusted to pH 6.7. It was assumed that MES did not react with the manganite surface or interfere with Pb sorption under the experimental conditions employed on the basis of previous studies (6). Aliquots were removed after 3 h of reaction time, filtered through 0.2 μm pore size membrane filters, and quenched with 12 μL of concentrated HNO₃. Concentrations of Pb and Mn in solution were measured using flame atomic absorption spectrometry (AAS) with detection limits of 4.8 μM and 5.5 μM, and under certain cases graphite furnace AAS was employed for measuring Pb with a lower detection limit of 0.24 μM.

Desorption experiments were conducted at 296 K by removing the equilibrium supernatant solution, replacing the solution with an equal volume of NaClO₄ background solution, and resuspending the Mn oxide solution mixture for the same reaction time as the adsorption isotherm experiments (3 h).

Chemisorption or specific adsorption energy (ΔG^o_{chem}) was estimated according to previous studies (27–30). The mean isotheric heat of adsorption at a given surface adsorption

density, ΔH_r (kJ mol⁻¹) was estimated with the Clausius–Clapeyron equation (31):

$$\Delta H_r = R \ln[(C_2/C_1)] / (1/T_2 - 1/T_1)$$

where R is the molar gas constant (kJ mol⁻¹ K⁻¹), C₂ (mol dm⁻³) is the equilibrium concentration of an ion at absolute temperature T₂ (K); and C₁ (mol dm⁻³) is the equilibrium concentration of an ion at absolute temperature T₁ (K).

XAFS Analyses. X-ray absorption fine structure (XAFS) spectra were collected at beamline X-11A at the National Synchrotron Light Source (NSLS) at Brookhaven National Laboratory, Upton, NY, to explore the chemical nature of Pb-reacted birnessite and manganite samples. The electron beam energy was 2.5 GeV, and Pb L_{III}-edge (13055 eV) spectra were collected in fluorescence mode using a Stern-Heald detector filled with Kr and an As filter to minimize elastic scattering of the samples and six sheets of Reynolds aluminum foil to minimize Mn–K_α background fluorescence. Samples were prepared in the glovebox using 10 g L⁻¹ birnessite and manganite, with initial concentrations of Pb to yield approximately similar loadings on the surface. Three scans (minimum) were collected per sample with the following scan settings: –200 to –30 eV (relative to the Pb edge) in 10 eV steps and 1 s count time; –30 to 30 in 0.5 eV steps at 1 s count time; 30 eV to 6 Å⁻¹ in 0.07 Å⁻¹ steps at 2 s count time; 6 Å⁻¹ to 11 Å⁻¹ in 0.07 Å⁻¹ steps at 5 s count time. Data reduction steps were performed using WinXAS 97 1.1. In extracting the χ(k) function, the XAFS signal was isolated from the absorption edge background by using a cubic spline function fit with seven segments. The k³-weighted χ(k) function was then Fourier transformed over k = 2–10 Å⁻¹ to yield the radial structure function (RSF). Data fitting was done in k space with a multishell fit routine and with an amplitude reduction factor (S₀²) fixed at 0.65. The FEFF 7.02 code reference (32) was utilized to calculate single scattering theoretical spectra and phase shifts for Pb–O and Pb–Mn backscatterers using an input file based on a structural model of α-PbO (33), with Pb atoms at 3.69 and 3.96 Å replaced by Mn.

Results and Discussion

Adsorption Kinetics. The kinetics of Pb sorption on birnessite were rapid, with 82% sorbed after 3 h (Figure 1). The sorption reaction slowly continued, with 86% removed from solution

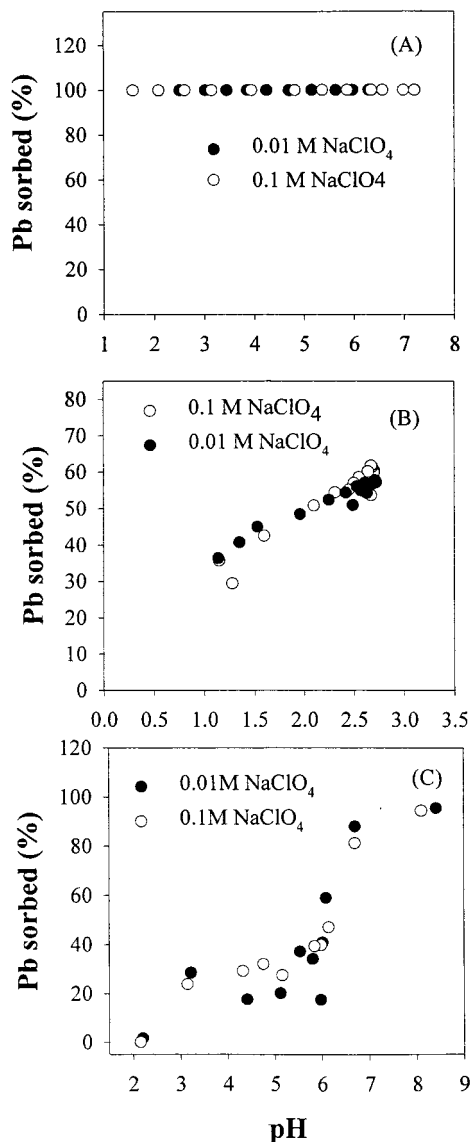


FIGURE 2. Ionic strength and pH edges at 296 K describing Pb(II) adsorption on (a) 1 g L^{-1} birnessite and initial $[\text{Pb}]_0 = 0.14 \text{ mM}$; (b) 1 g L^{-1} birnessite and $[\text{Pb}]_0 = 2.74 \text{ mM}$; (c) 0.1 g L^{-1} manganite and initial $[\text{Pb}]_0 = 14 \text{ }\mu\text{M}$.

after 24 h. More Pb was sorbed on birnessite at $23 \text{ }^\circ\text{C}$ than at $5 \text{ }^\circ\text{C}$ throughout the entire reaction period suggesting an endothermic reaction. Dissolved Mn release from birnessite was concurrent with Pb sorption. Kinetics of dissolved Mn release in the absence of Pb were measured and revealed negligible amounts of Mn in solution (not shown). To identify the source of displaced Mn in Pb-reacted birnessite, the structure of birnessite must be considered.

The structure of hexagonal birnessite is analogous to that of chalcophanite ($\text{ZnMn}_3\text{O}_7 \cdot 3 \text{ H}_2\text{O}$), where one out of seven Mn(IV) O_6 octahedral sites is vacant and interlayer Zn cations are located above and below the vacancies (34, 35). Layer charge deficiency of hexagonal birnessite is compensated by sorption of Mn(II), Mn(III), and H^+ in the interlayer (36, 37). The monoclinic form of birnessite (38) was shown recently to contain Mn(III) instead of layer vacancies (36, 37). It was assumed that the synthetic birnessite used in this study was structurally similar to hexagonal birnessite and this assumption was inherent to the Pb-EXAFS interpretation discussed below. The Mn species in the interlayer vacancy sites of birnessite were likely displaced from the structure by sorbed Pb that diffused into the interlayer, consistent with an

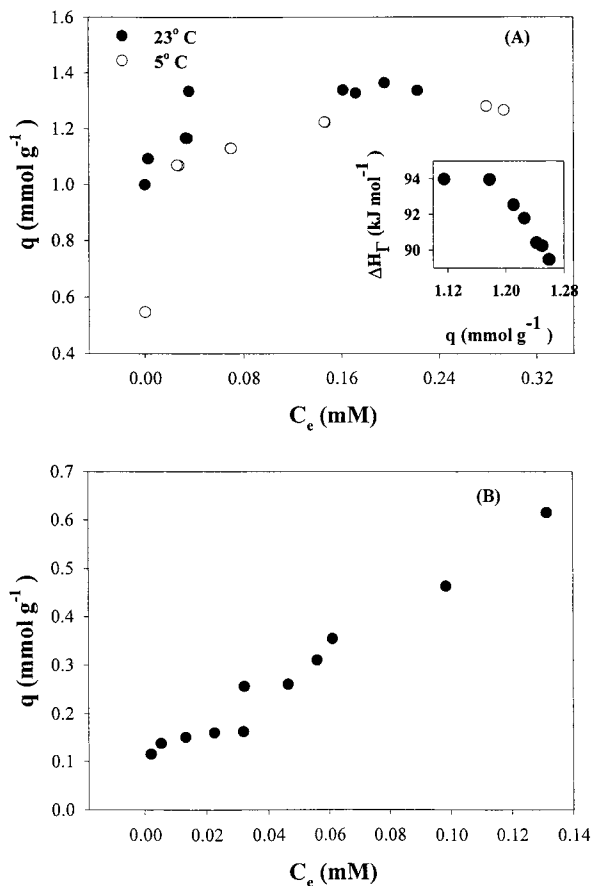


FIGURE 3. Pb(II) adsorption isotherms on (a) 1 g L^{-1} birnessite and $I = 0.01 \text{ M NaClO}_4$, as a function of temperature, with inset showing the isosteric heat of adsorption (ΔH_T) as a function of surface loading. (b) 0.1 g L^{-1} manganite and $I = 0.01 \text{ M NaClO}_4$.

endothermic process and the continued slower uptake at longer times (39, 40). The sorption of Pb on manganite was rapid and essentially complete after 3 h with no detectable release of Mn to solution (data not shown).

Ionic Strength Edges, pH Edges, and Isotherms. Strong sorption of Pb on birnessite was demonstrated by the high affinity over a wide pH range of 1.5–7.5 and the independence of ionic strength (Figure 2a). These findings agree with previous studies for Pb reactivity on birnessite (16, 17). Additional experiments at lower pH and higher initial Pb concentration indicated substantial sorption at and below the PZC of birnessite (Figure 2b). In contrast, a pH dependence was observed for Pb sorption on manganite, with a pH_{50} of ~ 6.0 that approximately corresponds to the PZC of the surface indicating that Pb may be sorbing to deprotonated surface functional groups (Figure 2c).

Representative adsorption isotherms describing Pb sorption on birnessite indicate a high affinity isotherm, resembling the H- or L-type isotherm with an adsorption maximum of $0.2 \text{ mol}_{\text{Pb}} \text{ mol}^{-1}_{\text{Mn}}$ (Figure 3a). In contrast, the Pb sorption isotherm was approximately linear ($r^2 = 0.97$) for manganite (Figure 3b) demonstrating the higher affinity of birnessite for Pb. More Pb was sorbed at $23 \text{ }^\circ\text{C}$ than $5 \text{ }^\circ\text{C}$ on birnessite in agreement with the kinetic data. The estimated isosteric heat of adsorption (ΔH_T) value of 94 kJ mol^{-1} at a surface density of 1.1 mmol g^{-1} indicated the adsorption process was endothermic, and the decrease in ΔH_T with surface coverage (inset, Figure 3a) suggested that birnessite has heterogeneous adsorption sites for Pb. Decreases in ΔH_T with surface coverage are commonly ascribed to surface heterogeneity (41). Benjamin and Leckie (39) proposed the het-

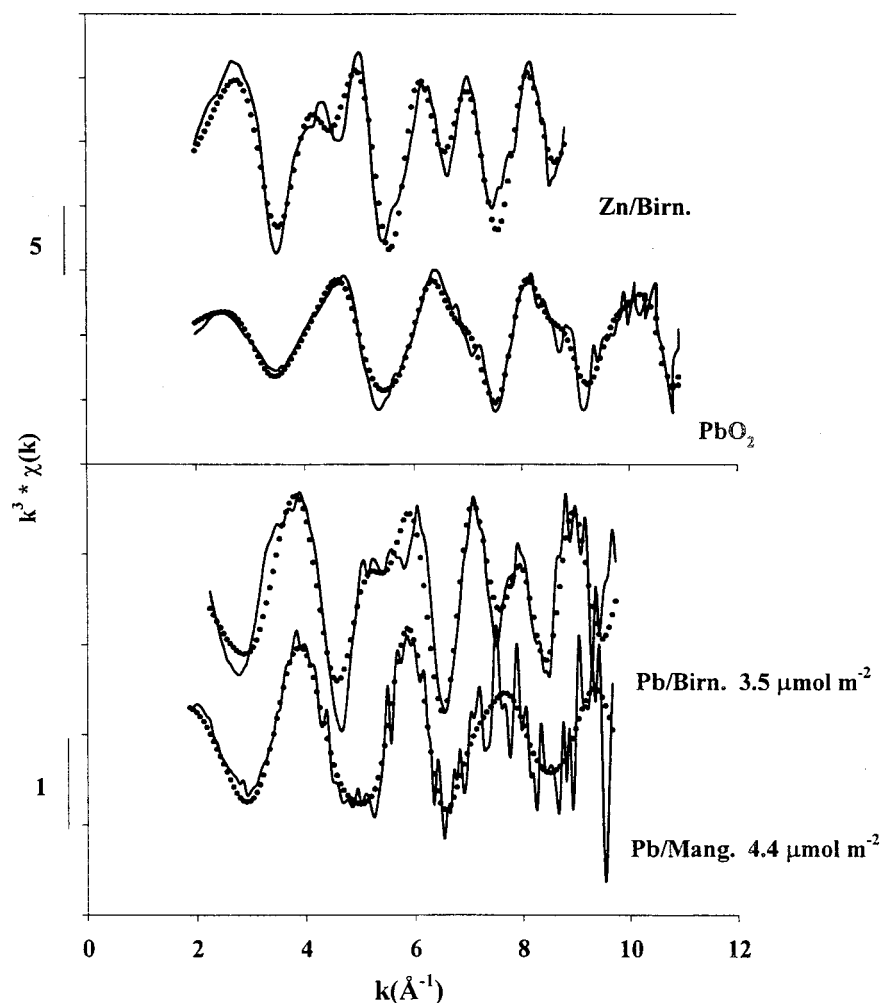


FIGURE 4. Experimental k^2 -weighted $\chi(k)$ functions derived from XAFS spectral analyses for Pb reacted with birnessite ($3.5 \mu\text{mol Pb m}^{-2}$) and manganite ($4.4 \mu\text{mol Pb m}^{-2}$) at 296 K and $I = 0.01 \text{ M NaClO}_4$ compared to Zn reacted with birnessite and a $\beta\text{-PbO}_2$ standard. The solid symbols represent multishell fits to the experimental data (solid lines). For Zn/birnessite and $\beta\text{-PbO}_2$ spectra, the scale is different because the first Me-O coordination shell is octahedral with $N = 6$.

erogeneous site binding model for amorphous iron oxyhydroxide and stated that the high energy sites were occupied first, followed by lower energy sites with a decrease in binding ability of the surface at higher adsorption densities. Further evidence for heterogeneous surface sites on birnessite was provided by modeling results of Catts and Langmuir (42). It was shown that birnessite possessed heterogeneous surface sites with a spectrum of binding energies for Pb, with the highest energy sites saturated at surface coverages of $<1\%$. The high energy sites could be the three oxygens surrounding each octahedral vacancy, recently modeled as a doubly charged sorption site, able to form tridentate inner-sphere complexes with metal ions (38).

The release of Mn(II) during Pb adsorption on birnessite was concentration dependent and $<1\%$ of adsorbed Pb was desorbed by background NaClO_4 at the highest loading (Table 1). This could be ascribed to an increase in the activation energy required to break the Pb–birnessite bond (40). More Pb was released from manganite than from birnessite at $\sim 0.1 \text{ mmol g}^{-1}$. Similarly, McKenzie (17) reported very little desorption of Pb from birnessite using 2.5% acetic acid with $>90\%$ nonextractable Pb after 1 d, and 95% after 28 weeks. Desorption of Pb from hydrous iron oxide and goethite was reported to be reversible with respect to pH with no apparent residence time effect (2, 43). Despite spectroscopic confirmation of a bidentate inner-sphere bonding mechanism between Pb and Al oxide surfaces, desorption of Pb was nearly

TABLE 1. Representative Pb Adsorption and Desorption Studies and Estimated Thermodynamic Parameters for Birnessite at pH 3.7 and Manganite at pH 6.7

solid-phase mineral	Pb adsorbed (mmol g^{-1})	Mn released (mmol g^{-1})	Pb desorbed (%)	ΔG_{chem}^0 (kJ mol^{-1})
birnessite	0.1	0	0	
	0.96	0.04	0	-83.6
	1.33	0.09	0.3	
manganite	0.14	0	6.2	
	0.26	0	100	-66.6

complete when desorption was allowed to reach equilibrium (6). Additional desorption studies for longer reaction times would be useful to further characterize Pb desorption behavior.

The thermodynamic driving force for Pb adsorption was greater on birnessite than on manganite based on the estimated magnitude of ΔG_{chem}^0 (Table 1), and this was reflected in the stronger Pb adsorption on birnessite observed in the pH edge and isotherm experiments. The ΔG_{chem}^0 values for Pb on birnessite and manganite exceeded those in previous investigations for Co(II), Mn(II), Ni(II), Zn(II), and Cu(II) adsorption on hydrous manganese dioxide, which ranged from -8 kJ mol^{-1} for Ni(II) to -20 kJ mol^{-1} for Co(II) (30, 44). Direct in situ spectroscopic evidence was obtained to explore the chemical nature of the adsorbed Pb and help

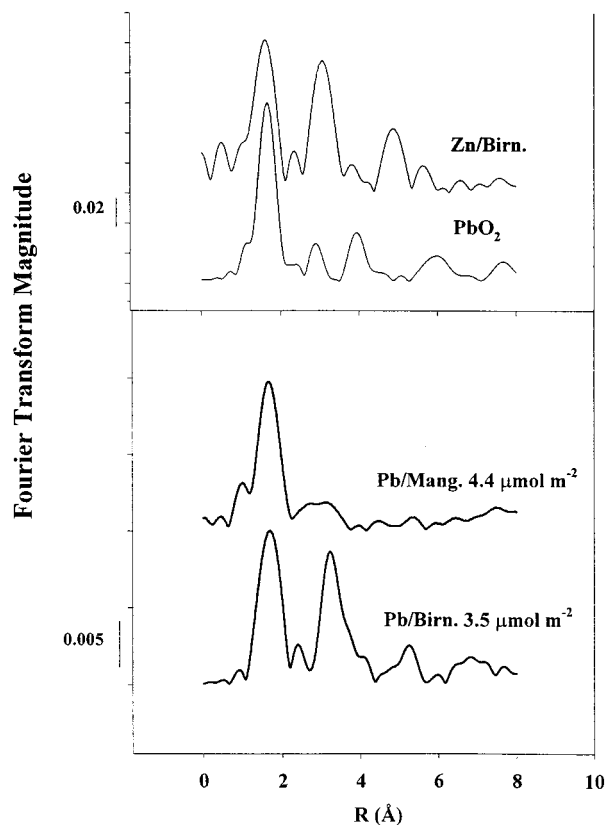


FIGURE 5. Radial structure functions (RSFs) of the chi functions in Figure 4, uncorrected for phase shift.

explain the slow release rate of Pb.

XAFS. Results of the XAFS experiments are shown in Figures 4 and 5. Spectral comparisons were made using Zn reacted with birnessite (Zn/Birn) as an analogue of chalcophanite to observe whether Pb partitioned to vacancy sites in birnessite, an approach used by others (21). Additionally, spectroscopic characterization of the two-electron oxidation product of Pb(II), β -PbO₂, was used to aid in determining the mechanisms of Pb removal on birnessite and manganite. The best fits of the k^3 -weighted $\chi(k)$ functions for Pb reacted with birnessite and manganite were achieved by fitting O in the first shell and Mn in the second shell (Figure 4). The raw χ data show differences for the Pb/birnessite and Pb/manganite samples, with a distinctly stronger beat pattern resulting from a greater contribution of Mn scattering in the birnessite sample as compared to that in the manganite sample (Figure 4). The strong beat pattern was also observed in Zn/birnessite. These findings were reflected in the radial structure functions (RSFs), which show a much higher Mn coordination of Pb sorbed to birnessite than Pb on manganite, and suggest that Pb and Zn were adsorbed at similar sites on birnessite based on the similarity of second shell Mn scattering (Figure 5).

Fitted bond lengths indicated that Pb reacted with birnessite and manganite was coordinated to surface groups with O as the ligating atom (O²⁻, OH⁻, or H₂O) in the first coordination shell with $R_{\text{Pb-O}} = 2.28$ – 2.32 Å (Table 2). The R and CN for the O shell of Pb sorbed to the solid Mn oxides described in this study are consistent with distorted trigonal pyramidal coordination of Pb(II) by hydroxide ions or oxygen atoms, first offered by Manceau et al. (45) and confirmed by Bargar et al. (46, 47). The first O shell of aqueous Pb(II) is characterized by a large Debye–Waller factor, indicating large disorder, and has a radial distance R of approximately 2.5 Å (10–12), far larger than the distance of about 2.3 Å for the adsorbed Pb on birnessite and manganite.

TABLE 2. Structural Parameters Derived from XAFS Analyses

sample	Me–O shell			Me–Mn shell			Pb–Pb shell		
	R(Å) ^{a,d}	N ^{b,e}	$\sigma^2(\text{Å}^2)^c$	R(Å) ^{a,d}	N ^b	$\sigma^2(\text{Å}^2)$	R(Å)	N	$\sigma^2(\text{Å}^2)$
Pb/birnessite	2.32	2.6	0.009	3.74	3.5	0.011			
Pb/manganite	2.28	2.3	0.008	3.31	0.7	0.01			
				3.87	0.7	0.01			
β -PbO ₂	2.15	5.8	0.003				3.38	2.3	0.004
							3.87	5.8	0.006
Zn/birnessite	2.07	5.4	0.005	3.50	6.3	0.006			

^a Interatomic distance. ^b Coordination number. ^c Debye–Waller factor. ^d Fit quality limits for parameters: ± 0.02 Å; ^e $\pm 20\%$; ^f ± 0.05 Å; ^g $\pm 40\%$.

The second shells evident in the RSF of the Pb/Mn oxide samples could be successfully fit only with Mn as the second neighbor. No evidence for Pb–Pb scattering was found, indicating that no oxidation products such as β -PbO₂ were present. The formation of β -PbO₂ would lead to Pb–Pb scattering, which, due to Pb being a strong backscatterer, should be quite pronounced if it occurred to a significant extent. The lack of Pb(II) oxidation was further confirmed by the radial distances for β -PbO₂ (first shell $R_{\text{Pb-O}} = 2.15$ Å) which reflected differences in the ionic radius for Pb(II) and Pb(IV) (Table 2) and the lack of stoichiometric Mn release to solution. The formation of other possible Pb precipitates, e.g. a mixed Pb–Mn hydroxide with low Pb content, cannot be entirely ruled out because of the limited k range of our EXAFS data. Such precipitates have, however, not been observed in studies of Pb sorption to Al and Fe(III)hydroxides (6, 46, 47).

The Pb–Mn distances found in the birnessite and manganite samples were used to determine the sorption mechanisms of Pb to these solid phases. The Pb/manganite sample clearly showed two Mn shells surrounding the central Pb atoms, consistent with Pb edge ($R_{\text{Pb-Mn}} = 3.31$ Å) and corner-sharing inner-sphere complexes ($R_{\text{Pb-Mn}} = 3.87$ Å) based on average Mn–O distances of 2.05 Å (48) and experimentally determined Pb–O distances of 2.3 Å (Table 2). These shells do not show up in the Pb/birnessite sample, which shows only one Mn shell at a radial distance different from those found in the manganite sample ($R_{\text{Pb-Mn}} = 3.74$ Å). This Pb–Mn radial distance on birnessite is interpreted as a corner-sharing Pb complex located above and below the vacancy sites (21, 22, 49) based on Mn–O distances for birnessite of 1.92 Å (38). Thus, the Pb–Mn distances found for the Pb/Mn oxide samples are likely consistent with Pb forming (mononuclear) adsorption complexes. We therefore interpret our data in terms of the formation of 2-dimensional mononuclear Pb adsorption complexes at the Mn oxide surfaces studied here.

The fitting results for the second shell (Pb–Mn scattering) show a higher DW factor and a lower CN for the Pb/birnessite sample as compared to those of the Zn/birnessite sample. This suggests a higher degree of disorder in the population of inner-sphere Pb complexes forming at the birnessite surface as compared to that of the Zn inner-sphere complexes. There is a longer correlation (likely due to multiple scattering) in the Pb/birnessite sample, as indicated by the peak in the radial structure function at about 5.3 Å (uncorrected for phase shift). Although both Pb and Zn adsorb to vacancy sites in birnessite, the resultant adsorption complexes of Pb appear to be more disordered than Zn.

These EXAFS data indicate that Pb(II) formed inner sphere complexes on birnessite and manganite with no evidence to suggest oxidation as an operative mechanism of Pb uptake. The release of dissolved Mn concurrent with Pb sorption and the similarity in Zn-birnessite and Pb-birnessite XAFS spectra indicated that Pb coordinated to vacancy sites in the

birnessite layer structure. The difference in Pb coordination between manganite and birnessite apparently explained the contrasting desorption behavior between the two Mn minerals. This could have significant implications for Pb behavior in the environment, particularly in soils containing solid-phase Mn(III,IV) (oxyhydr)oxides.

Acknowledgments

We thank the staff at beamline X-11A, D.R. Roberts for providing the XAFS data for the Zn-reacted birnessite, D.G. Strawn, and three anonymous reviewers for constructive reviews of the manuscript. C.J.M appreciates the support of a DuPont Graduate Fellowship.

Literature Cited

- (1) Sauv e, S.; McBride, M. B.; Hendershot, W. *Environ. Sci. Technol.* **1998**, *62*, 618–621.
- (2) Ainsworth, C. C.; Pilon, J. L.; Gassman, P. L.; Van Der Sluys, W. G. *Soil Sci. Soc. Am. J.* **1994**, *58*, 1615–1623.
- (3) Ma, Q. Y.; Logan, T. J.; Traina, S. J.; Ryan, J. A. *Environ. Sci. Technol.* **1994**, *28*, 408–418.
- (4) Ford, R. G.; Bertsch, P. M.; Farley, K. J. *Environ. Sci. Technol.* **1997**, *31*, 2028–2033.
- (5) Mart nez, C. E.; McBride, M. B. *Environ. Sci. Technol.* **1998**, *32*, 743–748.
- (6) Strawn, D. G.; Scheidegger, A. M.; Sparks, D. L. *Environ. Sci. Technol.* **1998**, *32*, 2596–2601.
- (7) Huang, J. W.; Chen, J.; Berti, W. R.; Cunningham, S. D. *Environ. Sci. Technol.* **1997**, *31*, 800–805.
- (8) Sparks, D. L. *Environmental Soil Chemistry*; Academic Press: San Diego, 1995.
- (9) Sparks, D. L., Ed. In *Soil Physical Chemistry*; CRC Press: Boca Raton, FL, 1999.
- (10) Bargar, J. R.; Towle, S. N.; Brown, G. E., Jr.; Parks, G. E. *Geochim. Cosmochim. Acta* **1996**, *60*, 3541–3547.
- (11) Bargar, J. R.; Brown, G. E., Jr.; Parks, G. E. *Geochim. Cosmochim. Acta* **1998**, *62*, 193–207.
- (12) Strawn, D. G.; Sparks, D. L. *J. Colloid Interface Sci.* **1999**, *216*, 257–269.
- (13) McKenzie, R. M. In *Minerals in Soil Environments*; Dixon, J. B., Weed, S. B., Eds.; Soil Science Society of America: Madison, WI, 1989.
- (14) Chorover, J.; Sposito, G. *Geochim. Cosmochim. Acta* **1995**, *59*, 875–884.
- (15) Jenne, E. A. *Adv. Chem. Ser.* **1968**, *67*, 337–387.
- (16) Gatte, R. R.; Laitinen, H. A. *Anal. Chem.* **1974**, *46*, 2022–2026.
- (17) McKenzie, R. M. *Aust. J. Soil Res.* **1980**, *18*, 61–73.
- (18) Cronan, D. S. In *The Sea*; Goldberg, E. D., Ed.; Wiley: New York, 1974.
- (19) Hem, J. D. *Chem. Geol.* **1978**, *21*, 199–218.
- (20) Manceau, A.; Charlet, L.; Boisset, M. C.; Didier, B.; Spadini, L. *Appl. Clay Sci.* **1992**, *201*–223.
- (21) Manceau, A.; Harge, J. C.; Bartoli, C.; Silvester, E.; Hazemann, J. L.; Mench, M.; Baize, D. In *Biogeochemistry of Trace Elements*; Iskandar, I. K., et al. Eds.; Berkeley, CA, 1997.
- (22) Morin, G.; Ostergren, J. D.; Juillot, F.; Ildefonse, P.; Calas, G.; Brown, G. E., Jr. *Am. Mineral.* **1999**, *84*, 420–434.
- (23) Bricker, O. *Am. Mineral.* **1965**, *50*, 1296–1354.
- (24) McKenzie, R. M. *Mineral. Mag.* **1971**, *38*, 493–502.
- (25) Murray, J. W. *J. Colloid Interface Sci.* **1974**, *46*, 357–371.
- (26) Giovanoli, R.; Leuenberger, U. *Helv. Chim. Acta* **1969**, *52*, 2333–2340.
- (27) Stumm, W.; Huang, C. P.; Jenkins, S. R. *Croat. Chem. Acta* **1970**, *42*, 223–245.
- (28) James, R. O.; Healy, T. W. *J. Colloid Interface Sci.* **1972**, *40*, 65–81.
- (29) Parks, G. A. In *Chemical Oceanography*; Riley, J. P., Skirrow, G., Eds.; Academic Press: London, 1975.
- (30) Murray, J. W. *Geochim. Cosmochim. Acta* **1975**, *39*, 505–519.
- (31) Chiou, C. T.; Shoup, T. D. *Environ. Sci. Technol.* **1985**, *19*, 1196–1200.
- (32) Rehr, J. J.; Mustre de Leon, J.; Zabinsky, S.; Albers, R. C. *J. Am. Chem. Soc.* **1991**, *113*, 5135–5140.
- (33) Leciejewicz, J. *Acta Crystallogr.* **1961**, *14*, 1304.
- (34) Wadsley, A. D. *Acta Crystallogr.* **1955**, *8*, 165–172.
- (35) Post, J.; Appleman, D. E. *Am. Mineral.* **1988**, *73*, 1401–1404.
- (36) Silvester, E.; Manceau, A.; Drits, V. A. *Am. Mineral.* **1997**, *82*, 962–978.
- (37) Drits, V. A.; Silvester, E.; Gorshkov, A. I.; Manceau, A. *Am. Mineral.* **1997**, *82*, 946–961.
- (38) Post, J. E.; Veblen, D. R. *Am. Mineral.* **1990**, *75*, 477–489.
- (39) Benjamin, M. M.; Leckie, J. O. *J. Colloid Interface Sci.* **1981**, *79*, 209–221.
- (40) Strawn, D. G.; Sparks, D. L. In *Biogeochemistry of Trace Elements*; Iskandar, I. K., et al. Eds.; Berkeley, CA, 1998.
- (41) Adamson, A. W. *Physical Chemistry of Surfaces*; Wiley-Interscience: New York, 1967.
- (42) Catts, J. G.; Langmuir, D. *Appl. Geochem.* **1986**, *1*, 255–264.
- (43) Eick, M. J.; Peak, J. D.; Brady, P. V.; Pesek, J. D. *Soil Sci.* **1999**, *164*, 28–39.
- (44) Murray, D. J.; Healy, T. W.; Fuerstenau, D. W. *Adv. Chem. Ser.* **1968**, *79*, 74–81.
- (45) Manceau, A.; Boisset, M. C.; Sarret, G.; Hazemann, J. L.; Mench, M.; Cambier, P.; Prost, R. *Environ. Sci. Technol.* **1996**, *30*, 1540–1552.
- (46) Bargar, J. R.; Brown, G. E., Jr.; Parks, G. E. *Geochim. Cosmochim. Acta* **1997**, *61*, 2617–2637.
- (47) Bargar, J. R.; Brown, G. E., Jr.; Parks, G. E. *Geochim. Cosmochim. Acta* **1997**, *61*, 2639–2652.
- (48) Kohler, T.; Armbruster, T.; Libowitzky, E. *J. Solid State Chem.* **1997**, *133*, 486–500.
- (49) Ostergren, J. D.; Brown, G. E., Jr.; Parks, G. E.; Tingle, T. N. *Environ. Sci. Technol.* **1999**, *33*, 1627–1636.

Received for review April 26, 2000. Revised manuscript received April 24, 2001. Accepted April 26, 2001.

ES0012164